Atmos. Chem. Phys. Discuss., https://doi.org/10.5194/acp-2018-825
Manuscript under review for journal Atmos. Chem. Phys.
Discussion started: 5 October 2018

Atmospheric Chemistry and Physics Discussions

Subsiding shells and vertical mass flux in warm cumulus clouds over land

Christian Mallaun[1], Andreas Giez[1], Georg J. Mayr[2], and Mathias W. Rotach[2]

[1]Deutsches Zentrum für Luft- und Raumfahrt (DLR), Flight Experiments, Oberpfaffenhofen, Germany
[2]University of Innsbruck, Institute of Atmospheric and Cryospheric Sciences, Innsbruck, Austria

Correspondence to: Ch. Mallaun
(christian.mallaun@dlr.de)

Abstract. The mass flux of air lifted within the updrafts of shallow convection was thought to be compensated outside the cloud through either large scale subsidence or stronger downdrafts in a thin shell surrounding the cloud. Subsiding shells were postulated based on large eddy simulation and are experimentally tested in this study for shallow convection over land. Isolated cumulus clouds were probed with a small research aircraft over flat land, mountains, in different wind situations and at different levels of the clouds. The subsiding shell varies considerably between individual cloud transects. A shell-like narrow downdraft region was present on at least one edge in 105 out of 191 transects and on both edges in 29 transects. However, the average over all cloud transects shows a narrow downdraft region outside the cloud boundaries. The ensemble-mean subsiding shell is narrower on the upwind side of the cloud, while it is at least half a cloud diameter wide and more humid on the downwind side. At least half of the upward mass transport in the cloud is compensated within a distance of 20 % of the cloud diameter. A shell is not uniform. Distinct regions of downdrafts and updrafts with high variability of the vertical wind are frequent and randomly distributed in the vicinity and also within the cloud. Based on these findings, a subsiding shell is, however, a valid concept to describe an ensemble of shallow cumulus clouds over land.

1 Introduction

Air in shallow cumulus clouds is transported towards higher regions of the atmosphere where it detrains from the cloud and mixes with environmental air. This is an effective way to vertically transport energy, heat and moisture from the surface to higher levels. Traditionally, large scale subsidence between the isolated cloud cells is regarded to be responsible for compensating the mass flux within the cloud (e.g. Stull, 1988). Heus and Jonker (2008) found a characteristic thin layer of a downward airflow outside of the simulated cumulus clouds by means of Large Eddy Simulations (LES), which they named the subsiding shell. This simple cloud process is sketched in Fig. 1.

A similar concept already appears in the cloud model of shallow cumulus clouds by Scorer and Ludlam (1953). They describe a region of downward motion in the wake of a rising bubble, which is caused by evaporation of the cloudy boundaries. With respect to the turbulence in the cloud they conclude, that the disturbances within the undiluted updrafts might be small compared to the wake region where violent eddies are dominating. Jonas (1990) found such significant downdrafts outside of growing cumulus clouds from airborne measurements, while these were missing in the decaying clouds. This is also confirmed by later

Atmos. Chem. Phys. Discuss., https://doi.org/10.5194/acp-2018-825
Manuscript under review for journal Atmos. Chem. Phys.
Discussion started: 5 October 2018

Atmospheric Chemistry and Physics Discussions

measurements (e.g. Rodts et al., 2003; Blyth et al., 2005).

Wang et al. (2009) investigated the mean dynamical properties of the cloud margin in shallow convection with a large number of cloud transects from aircraft measurements and confirm the subsiding shell as a distinct minimum of vertical velocity at the cloud boundaries. Mixing of cloud and environmental air leads to evaporative cooling, which is the source for the subsiding shell (Heus and Jonker, 2008; Abma et al., 2013; Katzwinkel et al., 2014). Even though the subsiding shell is rather thin, the covered area is significant as it surrounds the entire cloud. Therefore, the area of the shell is large enough to account for major parts of the downward mass flux in the cloud free environment, while the contribution of subsidence outside of the shell is less important. Jonker et al. (2008) calculated the fraction of mass compensation to be $80\,\%$ within a diameter of $400\,\mathrm{m}$ around a cumulus cloud. The ability of the clouds to condition the entire atmospheric boundary layer (ABL) is strongly reduced by these downdrafts. Additionally, it is an efficient way to bring air from the top of the cloud to its lateral boundaries, where it can entrain into the cloud. Consequently, this entrained air has properties from above the entrainment level. Wang and Geerts (2010) showed that the thermodynamic properties of the air in the vicinity of the cloud vary strongly with its horizontal distance from the cloud.

Most measurements discussed so far targeted shallow convection above the ocean (e.g. Heus and Jonker, 2008; Jonas, 1990; Katzwinkel et al., 2014), although this cumulus cloud type is also a common and characteristic phenomenon in the temperate and continental climate of the mid-latitudes. Wang et al. (2009) included shallow convection over land in their analysis, but restricted themselves to the mean properties of the cloud ensemble. In this study we present the results of 6 measurement flights over central Europe to test the validity of the subsiding shell concept for shallow convection over land. We investigate the mean distribution as well as individual cloud transects and discuss shallow convection for different synoptic situations and terrain.

In the following section we describe the assets and limitations of the instrumented aircraft and give an overview of the measurement campaign and methods. In Section 3 we show the results for some selected cloud transects and look at the distribution of the wind and thermodynamic properties of the individual cloud transects. This is followed by more general observations of the mean properties and variability of shallow cumulus clouds and especially the characteristics of the subsiding shell in Sect. 4. We discuss the importance of the subsiding shell with a focus on the downward mass flux in Sect. 5, before we end with the conclusions in Sect. 6.

2 Probing shallow convection and the subsiding shell

2.1 The research aircraft

For the in situ measurements we used a Cessna Grand Caravan 208B (Caravan), which is equipped with a meteorological sensor package (Mallaun et al., 2015). This small research aircraft combines several advantages for the investigation of small scale phenomena in the ABL such as the strong single engine power, high manoeuvrability and robust design. It is equipped with a high accuracy inertial reference system (IRS) for position and attitude determination and a meteorological sensor package mounted under the left wing. Mallaun et al. (2015) describe the details of the measurement instrumentation and the corre-

Atmos. Chem. Phys. Discuss., https://doi.org/10.5194/acp-2018-825
Manuscript under review for journal Atmos. Chem. Phys.
Discussion started: 5 October 2018

Atmospheric Chemistry and Physics Discussions

sponding uncertainties for the high-frequency 100 Hz measurements of pressure, temperature, humidity and wind vector. The main results of the measurement accuracy are summarized in Table 1.

2.2 The measurement campaigns

We conducted 6 measurement flights during two campaigns in June 2012 and July 2013 as listed in Table 2. Flights 1, 2 and 6 were conducted over relatively flat terrain north of the Alps and west of Munich, with smooth hills covered by fields and woodland. Flights 3 to 5 were devoted to the investigation of convective clouds over alpine topography. The flight tracks are shown in Figure 2 and information about the flight conditions can be found in Table 2.

We chose a similar flight strategy for all flights in order to achieve comparable data sets. Each flight started and ended with a vertical profile to obtain information about the undisturbed atmosphere outside the cloud. During ascent the cloud base and top were defined visually and a mean wind direction was estimated from the on-board quicklook data. With this information the operator defined the flight directions along and across the wind and up to three height levels within the cloud. In some cases also transects below cloud level were flown. Figure 3 shows the definitions of flight levels and directions as well as the main flight pattern, which is shaped like an 8. We also performed a simple reverse heading pattern, which allows for a high transect rate and facilitates the relocation of the target cloud. Beside the single cloud sampling we also performed longer straight flight legs in different directions and levels in order to gain broader statistics of the cloud properties.

2.3 Identifying clouds

The target clouds were selected visually during the flight. The identification of the cloud boundaries is realized in two steps. First, a digital time mark set by the operator during the flight gives a rough estimate of the location. As a second step, we take the signal of relative humidity to determine the exact cloud boundaries. Thus, *the cloud starts and ends with humidity saturation* as measured by a Ly-α absorption hygrometer (e.g. Bange et al., 2002), which has a response time faster than the acquisition frequency of 100 Hz.

We request a cloud diameter of at least 200 m to avoid very small cloud filaments. Such a cloud transect typically includes about 300 data points. This limit left us with 191 cloud transects including 17 different individual clouds which were repeatedly penetrated. Other authors have required different minimum cloud lengths. The scarce resolution of models or earlier measurements required higher thresholds of ≈ 500 m (e.g., Heus and Jonker, 2008; Jonas, 1990). More recent measurements, for example Wang et al. (2009) request a minimum length of 200 m or Katzwinkel et al. (2014) of 50 m.

Several factors complete the identification of a cloud. A single cloud often consists of more than one updraft. It can contain large gaps above its base, which makes it difficult to distinguish it from other clouds in the vicinity. Figure 4 a) shows an example. The cloud consists of an active updraft near the upwind side of the cloud separated by a gap at higher levels from an older, already decaying updraft further downwind, but joined through a common cloud base. For the data evaluation we have used the flight protocol and video tape to confirm the common cloud base. We also use a subset of 94 transects for which gaps in the transects above common cloud base were at most 150 m and less than 30 % of the cloud diameter. The cloud definition is summarized in Table 3. The existence of cloud gaps is in line with recent measurements (e.g. Jonas, 1990; Blyth et al., 2005;

Atmos. Chem. Phys. Discuss., https://doi.org/10.5194/acp-2018-825
Manuscript under review for journal Atmos. Chem. Phys.
Discussion started: 5 October 2018

Wang et al., 2009; Katzwinkel et al., 2014).

We classified the cloud transects in terms of cloud region (bottom, middle, top), along- or crosswind transects and terrain (lowland, mountains). A further criterion regards the activity status of the cloud, where we request a positive mean buoyancy inside the cloud for active clouds. The numbers of selected cloud transects representing the different criteria are listed in Table 4.

No agreement exists what constitutes a subsiding shell. Heus and Jonker (2008) originally defined a $50-100\,\mathrm{m}$ range of negative vertical wind directly outside the cloud. Wang et al. (2009) use a range of $50\,\mathrm{m}$ within and $200\,\mathrm{m}$ outside the cloud. Katzwinkel et al. (2014) split the subsiding shell in an inner and outer shell, where the inner shell has negative vertical velocities and negative buoyancy. It is driven by the negative buoyancy after mixing and evaporation at the cloud boundary (Abma et al., 2013) and thus, can partially also appear inside the cloud. The outer shell has still negative vertical velocity but positive buoyancy.

Based on these ideas we used the following criteria to identify a subsiding shell: In order to capture a high number of cases the width of the subsiding shell must be between $1\,\%$ and $20\,\%$ in cloud diameter. A downdraft exists within $5\,\%$ in cloud diameter outside of the cloud boundary. The subsiding shell can already start within the cloud. However, it must not have a length of more than $20\,\%$ in cloud diameter. This definition is summarized in Table 3. The median cloud length of the 191 transects is $\approx 1300\,\mathrm{m}$. Thus, the median subsiding shell has a length between $13\,\mathrm{m}$ and $260\,\mathrm{m}$ and starts within $65\,\mathrm{m}$ outside the cloud boundary. A possible part of this downdraft region inside the cloud is not longer than $260\,\mathrm{m}$. The length of the shell relative to the cloud diameter accounts for the high variability of cloud size. A circular subsiding shell with a length of $20\,\%$ in cloud diameter has an area approximately equal to the embedded cloud.

2.4 Computation of derived variables

2.4.1 Corrections of measurements in clouds

The presence of liquid water in the cloud modifies temperature and humidity measurements. Some of the liquid water evaporates as air is compressed in and in front of the total air temperature housing reducing the static temperature (T_s) and increasing the humidity mixing ratio (r) and thus the dewpoint temperature (T_d). We can estimate $T_d - T_s$ as the sum of evaporative cooling (ΔT_s) and the increased dewpoint temperature (ΔT_d) with

$$T_d - T_s = \Delta T_s + \Delta T_d = \frac{L_h \cdot \Delta r}{c_p} + \frac{\partial T_d}{\partial r} \cdot \Delta r, \tag{1}$$

as long as no significant sub- or supersaturation is present inside the cloud. The bias in water vapour mixing ratio (Δr) is equal to the evaporated amount of cloud water. In this approximation we use $L_h = 2.5\,\mathrm{MJkg^{-1}}$ for the standard enthalpy of evaporation and $c_p = 1005\,\mathrm{JK^{-1}kg^{-1}}$ for the heat capacity at constant pressure. The change of dewpoint temperature with the

Atmos. Chem. Phys. Discuss., https://doi.org/10.5194/acp-2018-825
Manuscript under review for journal Atmos. Chem. Phys.
Discussion started: 5 October 2018

Atmospheric Chemistry and Physics Discussions

change of mixing ratio ($\partial T_d/\partial r$) depends on pressure and temperature.

The humidity mixing ratio correction can be computed from Eq. 1,

$$\Delta r \approx (T_d - T_s) / \left(2.5\,\mathrm{K\,g^{-1}\,kg} + \frac{\partial T_d}{\partial r} \right), \tag{2}$$

if the mixing ratio is expressed in $\mathrm{g\,kg^{-1}}$, where $(T_d - T_s)$ is measured and the value for $\frac{\partial T_d}{\partial r}$ is calculated individually for each flight as listed in Table 5 following the common approximations for humidity conversion (e.g. Stull, 2000). The evaporation of Δr causes a cooling of the static temperature (ΔT_s) of

$$\Delta T_s = \frac{L_h \cdot \Delta r}{c_p} \approx 2.5\,\mathrm{K\,g^{-1}\,kg} \cdot \Delta r. \tag{3}$$

This correction rarely exceeds 1 K for the temperature and $0.4\,\mathrm{g kg^{-1}}$ for the mixing ratio.

However, when sensor wetting occurs as described by Lawson and Cooper (1990) and Wang et al. (2009), a cold peak can cause significantly larger errors especially outside the cloud and this correction does not work. On the Caravan two redundant temperature sensors (identical in construction) were available, which show different sensor wetting and thus, also different amplitudes of the cold peak. This allows for a very simple detection of the wetting effect. Consequently, for the investigation of the potential temperature and buoyancy distributions we have used just the first half of the transects in order to minimise the impact of sensor wetting. As the transects can start on either side of the cloud, the median distributions are available for the entire cloud transects, but contain a reduced set of data. The cold peak was often not visible in our measurements and the corrections defined in Eqs. 2 and 3 are applied to all data.

2.4.2 Computation of the buoyancy

The buoyancy is determined according to

$$B = g \left[\frac{\Theta_v'}{\overline{\Theta_v}} + (1-\kappa)\frac{p'}{\overline{p}} - r_l \right], \tag{4}$$

(Eq. 2.52, Houze (2014)) . To calculate the virtual potential temperature (Θ_v) in clouds, the LWC is additionally needed (i.e., $\Theta_v = \Theta(1 + 0.61 \cdot 10^{-3} r - 1 \cdot 10^{-3} r_l)$, with the liquid water mixing ratio (r_l) (Stull, 2000). Again, r and r_l are expressed in $\mathrm{g\,kg^{-1}}$. The LWC is not measured directly, thus, for the calculation we assume a value of $r_l = 0.4\,\mathrm{g kg^{-1}}$ for the regions with humidity saturation, which corresponds to a temperature difference of $\sim 0.15\,\mathrm{K}$. The results of Wang et al. (2009) indicate smaller values of LWC near the cloud margins and slightly higher ones in the updraft core.

Similar to Wang et al. (2009), we calculate the mean values ($\overline{\Theta_v}$) and mean pressure ($\overline{p}$) from the data of each cloud transect. The perturbation values (Θ_v', p') are then defined as the deviation from these mean values. Here, κ is the ratio of the gas constant and the specific heat capacity of air at constant pressure (i.e., $\kappa = R/c_p = (c_p - c_v/c_p)$) and g the acceleration due to gravity. The conserved variable Θ_v is used to compensate for inevitable height changes of the aircraft during the passage through the cloud. The pressure is altitude-corrected as described in Mallaun et al. (2015) with

$$p_{\mathrm{ref}} = p_0 \cdot e^{-\frac{g \cdot \Delta h}{R \cdot \overline{T}_v}}. \tag{5}$$

Atmos. Chem. Phys. Discuss., https://doi.org/10.5194/acp-2018-825
Manuscript under review for journal Atmos. Chem. Phys.
Discussion started: 5 October 2018

Atmospheric Chemistry and Physics Discussions

For p_0 we take the pressure at the starting point and $\overline{T_v}$ is the mean value of virtual temperature approximated by the mean values at the current position and the starting point, Δh is measured with the DGPS.

2.4.3 Computation of the vertical mass flux

In order to calculate the mean vertical mass flux (f_m) from the center of the cloud to the cloud boundary and the compensating downward directed mass flux outside of it, we adopt the formulation presented in Heus et al. (2009). We calculate the vertical mass flux for the relative distance (x) from the cloud boundary with

$$f_m(x) = \overline{\rho(x) \cdot w(x)} \cdot n(x). \tag{6}$$

$w(x)$ is the vertical velocity at a relative distance (x) from the cloud boundary and ρ the air density, the overbar denotes the mean value of all data points with a common x for the density and wind product. Thus, $x = 0$ is at the boundary, positive values are within the cloud with a maximum of $x = 0.5$ at the center of the cloud and negative ones in the surrounding shell. $n(x)$ represents the number of data points within the range of x. The accumulated mass flux (F_m)

$$F_m(x) = \int_{0.5}^{x} f_m(x')\,\mathrm{d}x' \tag{7}$$

measures the integrated upward flux of air inside the cloud and estimates the compensating downward mass flux outside. The limits of integration reach from the cloud center to x. In our analysis we consider only relative values of $f_m(x)$ and $F_m(x)$, which are scaled by their respective maximum values.

3 The subsiding shell in single cloud transects

3.1 The subsiding shell in an example cloud of a low-wind flight

First, we look at a series of particular cloud transects during flight 2. This helps to explain the methods and discuss the cloud characteristics and the occurrence of the subsiding shell for the chosen examples. On the flight day shallow convection formed around midday in a low-wind situation with weak high pressure influence. Compared to the other flight situations the horizontal wind and wind shear of $\approx 1\,\mathrm{ms^{-1}km^{-1}}$ were very weak at least up to the highest flight level. Figure 4 a) shows a narrow cloud turret, which grew fast above the broader and longer persisting cloud base. After $5-10\,\mathrm{min}$ the turret (the upper part of the cloud) dissolved in the relatively dry surrounding air and gave way to a new updraft, while the cloud base persisted. Figure 5 a) shows measurements along a crosswind transect flown in the upper part of another cloud. The relative humidity shows a compact cloud with small cloud gaps in the western part indicated by subsaturation. Here, also the vertical wind velocities are small compared to the eastern half where updrafts of up to $5\,\mathrm{ms^{-1}}$ are present. Also the buoyancy is increased in the updraft region, while the pressure perturbation is significantly negative in the dissolving (or decaying) part of the cloud.
Outside the cloud boundaries, a clear signal of sinking air with magnitudes up to $3\,\mathrm{ms^{-1}}$ is present. On the left boundary an $\approx 200\,\mathrm{m}$ wide region of downdrafts starts already within the cloud. This is the subsiding shell. On the right side the downdraft

region is $\approx 300\,\mathrm{m}$ wide with a distinct minimum about $150\,\mathrm{m}$ away from the cloud boundary followed by a weak subsidence region.

However, not all of the transects possess a subsiding shell. Figure 6 shows humidity and vertical wind for 4 different transects for the same cloud in north-south direction (along the main wind direction). From the video tape and operator's notes there is strong evidence that all cloud parts have a common base, even though rather large sub-saturated regions occur. These gaps occur very frequently when weaker decaying cloud parts and regions with stronger updrafts tend to line up along the mean wind direction. It is almost impossible to recognise the vertical wind structure from one transect to the other, which might be due to a high spatial/temporal variability and transient behaviour of the cloud. In panel c) and d) the main updraft might be the same, but for the rest of the transects the vertical velocity structures are different. This is similar for many transects in other clouds (not shown).

Figures 5 and 6 exemplify the large variations of strength and diameter or distance from the cloud boundaries of the subsiding shell. In some cases no subsiding shell exists at all. We also find strong regions of downdrafts near the cloud and also frequently within the cloud itself, especially in the vicinity of cloud gaps (see Fig. 6 c near position 0.25). There are also significant updrafts outside the cloud.

3.2 The subsiding shell in different conditions

Figures 4 b) and 5 b) show cloud examples during flight 1 with prevailing strong westerlies. Sharp gradients in the humidity profiles of the cloud transects are present at the cloud entry but on the opposite side the decrease of humidity is slower. The shape of the humidity signal is similar at different height levels but the diameter of the cloud decreases with height. It is hardly possible to identify any persisting structures in the vertical wind from one transect to the other. We found high variability of the vertical wind, especially inside the cloud, but also in its vicinity. In every transect we saw significant downdrafts. However, these downdrafts are usually not connected to the cloud boundaries, but seem to be randomly distributed. Just in some transects we found a signal similar to a subsiding shell on either side of the cloud.

The clouds sampled in flights 3 to 5 developed above mountain peaks during strong high pressure influence with weak southerly wind. The convection tended to start above distinct points above the mountain ridges drifting north during its life cycle. However, in terms of downdraft regions in and near the clouds the same high variability is found as for the clouds over flat terrain.

Altogether, we investigated the shell properties for 191 cloud transects based on the definition in Table 3. For this analysis a running average of $0.5\,\mathrm{sec}$ is applied to the vertical wind data to eliminate small scale turbulent fluctuations. The results are summarized in Table 6. Only some of the investigated cloud transects (29 cases) possess a subsiding shell on both sides of the cloud. About half the cloud transects have a subsiding shell on the upwind side and approximately $30\,\%$ on the downwind or crosswind sides. The majority of the cloud transects on the downwind and crosswind sides of the cloud show a vast downdraft region near the cloud boundaries, which usually begins well within the cloud. The downdraft measured within the subsiding shell (if present) is usually not representing the absolute minimum of the vertical wind found in and around the cloud.

We find 105 cloud transects with either one or two subsiding shells. We do not find an obvious correlation between the subsiding

shell occurrences and the activity status of the clouds. There are slightly more shells found in clouds over flat terrain than over the mountains and more in the bottom and top levels compared to the mid level transects. The number of occurrences and the respective cloud properties are listed in Table 4.

4 Properties of the cumulus clouds and the subsiding shells

In the previous section we tested 191 different cloud transects on the existence of a subsiding shell. All these transects build a large sample to investigate the statistical distribution of the characteristic cloud properties. The boundaries of the clouds are estimated by the humidity distribution. Thus, the dynamical properties in the focus of the following discussion are independent of the cloud definition.

4.1 Distributions of wind, pressure, buoyancy and massflux

Figure 7 shows the median vertical velocity distribution for all the cloud transects. Note that the spatial coherence of the individual transects is lost with the representation of the percentiles. The median vertical velocity has a distinct maximum within the cloud, which is slightly shifted towards the upwind side. The vertical velocity becomes already negative well within the cloud. Thus, the average cloud boundary experiences downward motion. The minimum slightly outside of the cloud boundaries is stronger on the downwind side. Further away from the cloud the downdrafts become weaker. The 75 and 90 percentiles have no downdrafts at all while the 10 and 25 percentiles show continuous negative vertical velocity. The minimum near the cloud boundary is visible for all percentiles.

Figure 8 shows the median vertical wind distribution for different cloud categories stratified by cloud activity, level within cloud, underlying terrain and along or crosswind transects. Note that sample sizes vary. Active clouds have pronounced updraft regions and a subsiding shell at the boundaries. The minimum at the cloud boundaries is missing at the active bottom level, which might be due to the small sample available. The strongest updrafts are found for at cloud top level. The most distinct downdraft regions at the cloud boundaries are present on the downwind side of the transects of the center level and the clouds above mountains. They have a broad region of sinking air, which already starts well within the cloud. The active crosswind transects show these minima as well and half a cloud diameter of the boundary the vertical wind almost vanishes. This is in contrast to the active alongwind transects. On the upwind side they have almost no downdrafts with a very narrow minimum right outside the cloud boundary. On the downwind side the change of the vertical wind is small compared to the crosswind transects. The inactive transects show high variability of the wind signals inside and outside of the cloud. At cloud mid and top level they do not show any strong updrafts.

Figure 9 shows the histograms of the vertical velocity inside the cloud and within $20\,\%$ outside of the cloud diameter. The distributions obviously differ in size and shape, with some statistical values summarized in Table 7. In the cloud the mean vertical velocity is $\approx 0.5\,\mathrm{m/s}$ and the skewness of the distribution is directly visible in the figure with increased frequencies of fast rising parcels. However, only one of the selected transects has no negative vertical velocity at all within the cloud. Except of 8 cases all the transects have downdrafts stronger than $-1\,\mathrm{m/s}$ inside the cloud. In the shell the mean vertical velocity is

significantly below zero for all four cloud boundaries. Especially on the upwind side the distribution is narrow compared to the other investigated parts. In the downwind and crosswind shells we find stronger downdrafts and higher variability compared to the upwind side. The highest variability of the vertical velocity is present within the clouds, which is also visible in Fig. 7. In Fig. 9 a) the stronger downdrafts in the downwind shell compared to the upwind shell become visible. The frequencies and magnitude of the updrafts are similar for the shell region on both sides. A separated analysis of the left and right crosswind shells does not lead to any significant differences neither for the median distributions nor for the histograms.

Figure 10 presents the median distribution of the vertical mass flux and horizontal alongwind perturbation as well as the buoyancy and the horizontal pressure perturbation for the 191 selected cloud transects. The vertical mass flux in panel a) is calculated with Eq. 6, which leads to a very similar distribution and magnitude as the vertical velocity. Mathematically, the vertical wind signals are weighted with the air density, which in the most cases lies near $1\,\mathrm{kg\,m^{-3}}$. Similar to the vertical wind also the vertical mass flux is continuously negative for the 10 and 25 percentiles. Also the downward directed mass flux is strongest just outside of the cloud boundaries. The mean horizontal wind component along the flight track (u_{ac}) in Fig. 10 b) is significantly reduced within the cloud, where also the strongest updrafts are found. For the 10 and 25 percentiles this signal is most pronounced. It is enhanced on the upwind side and matches the mean values on the downwind side. This feature is only present in the alongwind transects, while it is not visible in the crosswind transects. It is strongest in the bottom level transects and vanishes in the top level (not shown). The distribution of u_{ac} is also characterized by a high variability which is similar to the vertical wind variability.

Figure 10 shows that within the cloud a mean upward motion coincides with enhanced buoyancy, while on both sides outside of the cloud the buoyancy is almost zero on average. On the upwind side a weak negative peak is indicated with a strong and clear gradient through the cloud boundary. This gradient is much weaker on the downwind side of the cloud, where values near zero are present well within the cloud. A similar feature is also visible in the relative humidity data (not shown), where the median value is significantly enhanced on the downwind side for at least half a cloud diameter. The median pressure perturbation (Fig. 10 d) is small and with magnitudes of a few Pascals similar to the sensor resolution ($= 2\,\mathrm{Pa}$). A weak negative anomaly is visible within the cloud, which is counteracted by positive contribution especially on the upwind side of the cloud. However, the percentiles show that significant deviations of the hydrostatic equilibrium are frequent both inside and outside of the clouds.

4.2 Sensitivity of the results

Even though the clouds are actively chosen during the flight with a focus on vital clouds, many of them contain big cloud gaps. Different rising plumes, decaying cloud parts with strong downdrafts and also subsaturated air parcels entrained into the cloud coexist and build the entity of a single cloud. From the chosen cloud transects 9 cases have no cloud gaps at all. For 25 cases the fraction of cloud gaps relative to the cloud diameter exceeds $50\,\%$. For the 25 percentile, the median and the 75 percentile we estimate a cloud fraction of $\approx 10\,\%$, $\approx 20\,\%$ and $\approx 40\,\%$, respectively.

In order to judge the robustness of the results in terms of cloud definition, we have repeated the analyses for the stricter criteria including restriction 4 and 5 as defined in Table 3. Thus, we omit the transects with a fraction of cloud gaps of more than $30\,\%$ or a cloud gap exceeding $150\,\mathrm{m}$. For the new analysis we select the more homogeneous clouds and neglect the less active or

complexer ones, that just 94 out of 191 cloud transects remain. In Table 4 the numbers of total occurrences are listed by the numbers in brackets. The frequencies of the subsiding shell remain very similar for the active transects. Just one subsiding shell is found for the inactive cases, which might be due to the small number of transects. In Figures 7 and 10 a) the respective median distribution for the reduced sample of 94 'ideal' clouds is represented by the green lines. It is obvious, that neglecting the less active clouds leads to stronger updrafts. However, the distribution at the cloud boundary and in the cloud free region remains almost unchanged. Also the histograms of the vertical velocity (not shown) remain qualitatively unchanged. The frequencies of the vertical velocities within the cloud are shifted towards higher values. The vertical velocity distribution in the shell regions are narrower compared to the results in Fig. 9. After all, the selection of the clouds is not substantially changing the results.

5 Discussion

The median vertical velocity distribution around shallow convection presented in Fig. 7 agrees well with results of former analyses of the subsiding shell (e.g. Heus and Jonker, 2008; Wang et al., 2009; Katzwinkel et al., 2014). The vertical velocity possesses a distinct minimum directly outside of the cloud boundaries, which is associated with a thin shell of sinking air covering the entire cloud. Figure 11 shows the relative vertical mass flux (f_m) and the relative accumulated mass flux (F_m) from the cloud center outwards. The maximum of mass flux is found well within the cloud, while a distinct minimum exists right outside of the cloud boundary. The downward flux in the shell has almost the same strength as the upward flow in the main updraft region. Half of the downward mass flux along the transect occurs within a distance of $20\,\%$ of the cloud diameter outside of the cloud. After half a cloud diameter the mass flux in the cloud is compensated. Both distributions of f_m and F_m are very similar to the observations of Heus et al. (2009), even though our manually selected clouds over land often have complex structures and include cloud gaps. Different from their results the vertical mass flux becomes negative already well within the cloud where already a significant portion of downward mass flux occurs. There is no significant change in the results, when we restrict the analysis from all the 191 cases to the 130 alongwind transects as shown by the grey dashed lines in Fig. 11 or to the crosswind transects (not shown).

So far, our results corroborate the findings of Heus et al. (2009). However, care must be taken when interpreting the mean distributions of cloud and shell properties. While a significant downdraft anomaly - the subsiding shell - is present in the median vertical wind distribution (see Fig. 7), this is not a characteristic feature of each individual cloud. Only 12 cloud transect of the 94 'ideal' cases and 29 transects of the entire 191 cloud transects have the 'narrow' region of sinking air on *both* sides of the cloud. About half of the cloud transects have a subsiding shell at least at one boundary (see Table 4), even though the criteria are chosen rather generously compared to Heus and Jonker (2008). There is a strong variability of the vertical wind outside of the clouds and the position of the downdrafts (and also updrafts). The presence of a subsiding shell depends on the current position of the downdrafts near the evolving cloud as the example in Fig. 6 shows. Downdrafts are frequent also inside the cloud and have a significant influence on the mass flux. About one third of the upward directed mass flux is already compensated inside the cloud by the downdrafts.

In the cloud, the regions of subsaturation (cloud gaps) tend to have negative vertical velocities. About $75\,\%$ of the data points

in cloud gaps have a negative vertical velocity with a mean of $-0.8\,\mathrm{ms}^{-1}$. We find a positive correlation of vertical wind and buoyancy (i.e., $r \approx 40\,\%$). Near the cloud gaps this indicates mixing of cloud air with environmental air. Recently, Yang et al. (2016) also observed small scale updrafts and downdrafts as characteristic feature in isolated cumulus clouds.

As a main conclusion from the analysed cloud transects over land, we do not find either the subsiding shell nor subsidence as a characteristic feature of the vertical wind near *individual* clouds (see Fig. 6). Although downdrafts are frequent near the cloud boundaries and also within the cloud itself, they do not necessarily form a coherent shell around the cloud surface. Instead, these downdrafts often alternate with updrafts of similar strength and diameter. The consecutive legs in Fig. 6 show how fast the wind structures change around the evolving cloud. They thus resemble turbulent eddies, which can be responsible for vertical mass transport as well as entrainment of environmental air into the cloud. However, the 'subsiding shell' is a valid concept for *ensembles* of clouds as shown in Fig. 7. According to Fig. 8 subsiding shells are typical for active clouds, most pronounced in the center and top cloud regions or for the crosswind transects. Subsiding shell are more pronounced for the transects over the mountains compared to the flat land. On the downwind side of active clouds the broad region of downdrafts is explainable by a humidity halo as observed by Perry and Hobbs (1996). Our results show, that the mass transport in the cloud is compensated within half a cloud diameter away from the cloud border. This has strong implications for the distribution and mixing of the cloud air in the environment. Compared to the concept of a downward mass flux via subsidence (Stull, 1988), less mixing and less transport of heat and energy occur. The mixing of cloud air in the upper ABL is reduced when the air stays near the cloud and directly sinks down in the subsiding shell to lower regions. Thus, the 'subsiding shell' has to be considered in a parametrisation scheme for shallow convection over land.

6 Conclusions

A series of cloud transects measured with a research aircraft were analysed with a special focus on the dynamical properties near the cloud boundaries. Former LES model results had shown a narrow coating downdraft region around shallow convective clouds, which is called a subsiding shell.

To test whether subsiding shells can be observed for shallow convection over land, we conducted 6 measurement flights in the years 2012 and 2013. It was possible to probe single clouds over flat land and mountain ridges, in different heights and different synoptic situations. The aircraft measured the thermodynamic properties of the clouds with the exception of liquid water content. A correction is presented for the temperature and humidity bias that occurs due to droplet evaporation inside the clouds. The target clouds were actively selected during the flights in order to choose well-defined vital clouds. For the investigation we manually selected 191 cloud transects. The clouds are usually not homogeneous masses of cloud air with a central main updraft but more complex formations with regions of updrafts, downdrafts and cloud gaps within one cloud. With a stricter cloud definition we repeated the analysis with a reduced cloud sample of 94 'ideal' clouds for a sensitivity test.

The median vertical velocity of the selected cloud transects shows a very similar distribution compared to the LES model results. We also do not see any significant differences between our measurements over land surface compared to earlier results from shallow convection over sea. The main feature in the distribution is a distinct minimum in the vertical wind immediately

outside of the cloud boundaries. A distinct downdraft on the downwind side starts well within the cloud and is wider compared to the upwind side, where the gradients of vertical velocity and buoyancy are stronger. A strong downward mass flux is present in the region of the subsiding shell, which compensates for a large fraction of the positive vertical mass transport within the cloud. Within a distance outside the cloud of $\approx 20\,\%$ in cloud diameter half of the upward directed vertical mass flux is compensated.

On the other hand, individual cloud transects do not usually possess a subsiding shell as defined in Table 3. Just 29 of the 191 investigated cloud transects have a subsiding shell on both boundaries and 105 transects on at least one side. In general, the distribution of the vertical wind is qualitatively similar over flat land and mountainous terrain, but there are quantitative differences. Active clouds have larger vertical velocity and vertical mass flux than inactive clouds. The strongest updrafts are present in the upper level and crosswind transects, while the downdrafts are most pronounced at the center level and mountain transects.

Strong downdrafts are frequent in the vicinity of the cloud boundaries, which leads to the characteristic feature of a subsiding shell in the mean vertical velocity profile. The individual cloud transects are characterized by strong updrafts and downdrafts both, inside and outside the cloud. They seem rather randomly distributed and resemble turbulent eddies, which are much smaller than the cloud diameter. An investigation of size, turbulence statistics and scaling with the cloud size in future research is desirable to understand the dynamics of shallow convection over land. Still, the concept of the subsiding shell seems a valid concept for mean properties of shallow convection over land with all its implications on the cloud air mixing and entrainment of upper level air into the cloud. The downdraft in the subsiding shell is able to account for a major part of the downward mass flux, which is compensating the net upward mass flux in the cloud. In contrast to subsidence in a large area between the clouds this process reduces the horizontal mixing of cloud air in the upper boundary layer, but keeps the cloud air in the near vicinity of the cloud itself.

Data availability. Data on personal request

Competing interests. All authors declare that they have no competing interests.

Acknowledgements. We thank the DLR flight crew for their enthusiastic commitment while circling in narrow turns around the target clouds. We thank the air traffic authorities in Germany and Austria for their support, which gave the permission to freely sample the clouds in these regions of high air traffic.

References

Abma, D., Heus, T., and Mellado, J. P.: Direct Numerical Simulation of Evaporative Cooling at the Lateral Boundary of Shallow Cumulus Clouds, J. Atmos. Sci., 70, 2088–2102, http://dx.doi.org/10.1175/JAS-D-12-0230.1, 2013.

Bange, J., Beyrich, F., and Engelbart, D. A. M.: Airborne measurements of turbulent fluxes during LITFASS-98: Comparison with ground measurements and remote sensing in a case study, Theoretical and Applied Climatology, 73, 35–51, http://dx.doi.org/10.1007/s00704-002-0692-6, 2002.

Blyth, A. M., Lasher-Trapp, S. G., and Cooper, W. A.: A study of thermals in cumulus clouds, Quarterly Journal of the Royal Meteorological Society, 131, 1171–1190, http://dx.doi.org/10.1256/qj.03.180, 2005.

Heus, T. and Jonker, H. J. J.: Subsiding Shells around Shallow Cumulus Clouds, J. Atmos. Sci., 65, 1003–1018, http://dx.doi.org/10.1175/2007JAS2322.1, 2008.

Heus, T., J. Pols, C. F., J. Jonker, H. J., A. Van den Akker, H. E., and H. Lenschow, D.: Observational validation of the compensating mass flux through the shell around cumulus clouds, Quarterly Journal of the Royal Meteorological Society, 135, 101–112, http://dx.doi.org/10.1002/qj.358, 2009.

Houze, R. A. J.: Cloud Dynamics, vol. 104, Academic Press, 2nd edition edn., 2014.

Jonas, P.: Observations of cumulus cloud entrainment, Atmospheric Research, 25, 105 – 127, https://doi.org/http://dx.doi.org/10.1016/0169-8095(90)90008-Z, 1990.

Jonker, H. J. J., Heus, T., and Sullivan, P. P.: A refined view of vertical mass transport by cumulus convection, Geophys. Res. Lett., 35, L07 810–, http://dx.doi.org/10.1029/2007GL032606, 2008.

Katzwinkel, J., Siebert, H., Heus, T., and Shaw, R. A.: Measurements of Turbulent Mixing and Subsiding Shells in Trade Wind Cumuli, J. Atmos. Sci., 71, 2810–2822, http://dx.doi.org/10.1175/JAS-D-13-0222.1, 2014.

Lawson, R. P. and Cooper, W. A.: Performance of Some Airborne Thermometers in Clouds, J. Atmos. Oceanic Technol., 7, 480–494, http://dx.doi.org/10.1175/1520-0426(1990)007<0480:POSATI>2.0.CO;2, 1990.

Mallaun, C. and Giez, A.: The Missing Link: How to optimize pressure calibration using the tower flyby method, in: 24th Annual SFTE EC Symposium, http://elib.dlr.de/95001/, 2013.

Mallaun, C., Giez, A., and Baumann, R.: Calibration of 3-D wind measurements on a single-engine research aircraft, Atmospheric Measurement Techniques, 8, 3177–3196, https://doi.org/10.5194/amt-8-3177-2015, 2015.

Perry, K. D. and Hobbs, P. V.: Influences of Isolated Cumulus Clouds on the Humidity of Their Surroundings, J. Atmos. Sci., 53, 159–174, http://dx.doi.org/10.1175/1520-0469(1996)053<0159:IOICCO>2.0.CO;2, 1996.

Rodts, S. M. A., Duynkerke, P. G., and Jonker, H. J. J.: Size Distributions and Dynamical Properties of Shallow Cumulus Clouds from Aircraft Observations and Satellite Data, J. Atmos. Sci., 60, 1895–1912, http://dx.doi.org/10.1175/1520-0469(2003)060<1895:SDADPO>2.0.CO;2, 2003.

Scorer, R. S. and Ludlam, F. H.: Bubble theory of penetrative convection, Quarterly Journal of the Royal Meteorological Society, 79, 94–103, http://dx.doi.org/10.1002/qj.49707933908, 1953.

Stull, R. B.: An introduction to Boundary Layer Meteorology, Kluwer Academic Publishers, 1988.

Stull, R. B.: Meteorology for Scientists and Engineers, Brooks/Cole, 2 edn., 2000.

Wang, Y. and Geerts, B.: Humidity variations across the edge of trade wind cumuli: Observations and dynamical implications, Atmospheric Research, 97, 144 – 156, https://doi.org/http://dx.doi.org/10.1016/j.atmosres.2010.03.017, 2010.

Atmos. Chem. Phys. Discuss., https://doi.org/10.5194/acp-2018-825
Manuscript under review for journal Atmos. Chem. Phys.
Discussion started: 5 October 2018

Wang, Y., Geerts, B., and French, J.: Dynamics of the Cumulus Cloud Margin: An Observational Study, J. Atmos. Sci., 66, 3660–3677, http://dx.doi.org/10.1175/2009JAS3129.1, 2009.

Yang, J., Wang, Z., Heymsfield, A. J., and French, J. R.: Characteristics of vertical air motion in isolated convective clouds, Atmospheric Chemistry and Physics, 16, 10 159–10 173, http://www.atmos-chem-phys.net/16/10159/2016/, 2016.

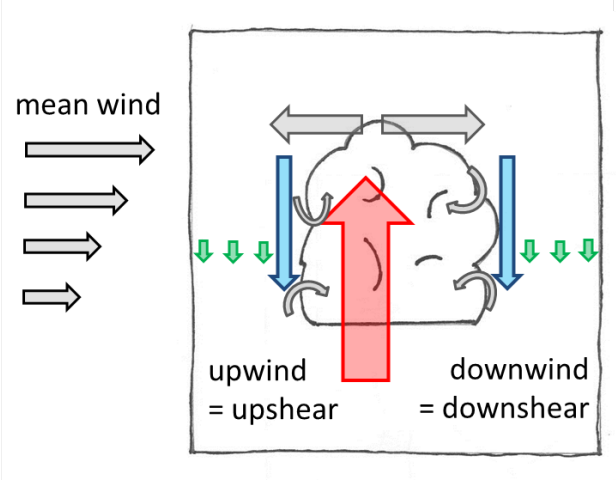

Figure 1. Conceptual model of a small cumulus cloud. The vertical mass flux within the cloud (red arrow) is compensated either through large scale subsidence (green arrows) or in the subsiding shell (blue arrows). Grey arrows indicate detrainment above the cloud and entrainment on the lateral cloud boundaries.The main updraft is shifted towards the upshear cloud boundary.

Atmos. Chem. Phys. Discuss., https://doi.org/10.5194/acp-2018-825
Manuscript under review for journal Atmos. Chem. Phys.
Discussion started: 5 October 2018

Atmospheric Chemistry and Physics Discussions

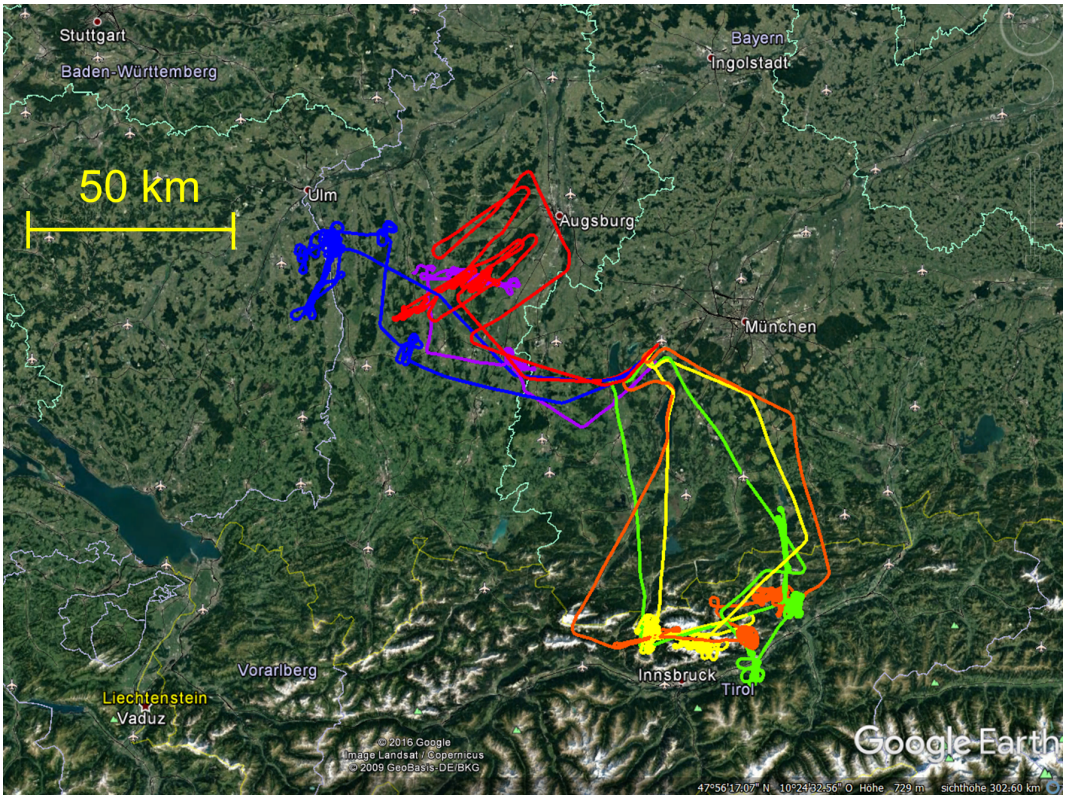

Figure 2. Overview of the target region for the measurement flights above the northern Limestone Alps and foothills west of Munich. The lines show the 6 flights listed in Table 2 colored blue, red, orange, yellow, green and purple, respectively. The thin yellow line marks the border between Austria and Germany (2016 Google, Image Landsat / Copernicus).

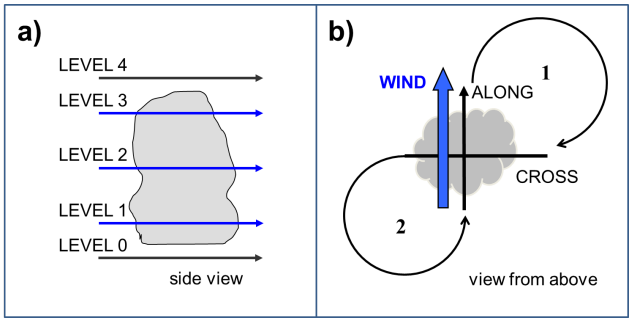

Figure 3. Definition of the chosen levels (a) and directions (b) during the measurement flights. The turns 1 and 2 in panel (b) indicate the main flight pattern resembling the number '8', which results in repeated flight transects along and cross the mean wind.

Atmos. Chem. Phys. Discuss., https://doi.org/10.5194/acp-2018-825
Manuscript under review for journal Atmos. Chem. Phys.
Discussion started: 5 October 2018

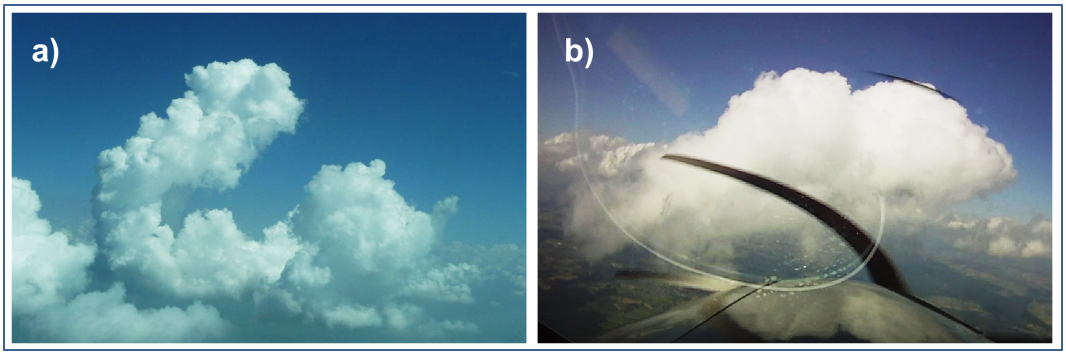

Figure 4. Examples of clouds in weak and strong shear environments, respectively. (a) Cloud in weak-wind, weak-shear environment during flight 2. Common cloud base in a humid surrounding with $rh > 85\,\%$, but cloud gaps in the upper part, which is surrounded by drier air $rh \approx 60\,\%$. Weak winds blow in the lower cloud part with $\approx 2 - 4\,\mathrm{ms}^{-1}$, the inclination of the cloud top indicates increasing wind with height. (b) Cloud in a boundary layer with strong wind shear during flight 1 immediately before a crosswind transect. The wind blows from the left and the shear-induced declination of the cloud is visible. The cloud bottom does not show a sharp line, which indicates that the cloud has reached at least a mature state, without a strong updraft in the lower cloud parts.

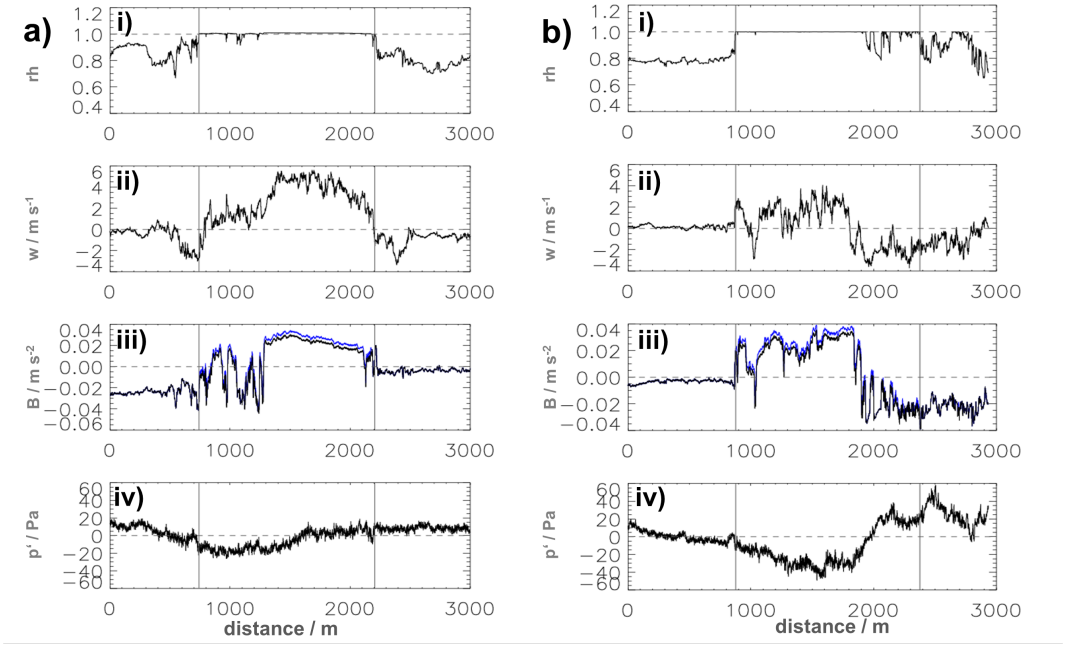

Figure 5. a) Measurement values for a crosswind transect through an active cloud during flight 2 looking downwind. The cloud boundaries are marked by the grey vertical lines. Panel (i) shows relative humidity; (ii) vertical wind; (iii) buoyancy based on a mean LWC of $0.4\,\mathrm{gm}^{-3}$, the blue line is buoyancy without the contribution of LWC and (iv) the horizontal pressure perturbation. b) Same for an alongwind transect during flight 1.

Atmos. Chem. Phys. Discuss., https://doi.org/10.5194/acp-2018-825
Manuscript under review for journal Atmos. Chem. Phys.
Discussion started: 5 October 2018

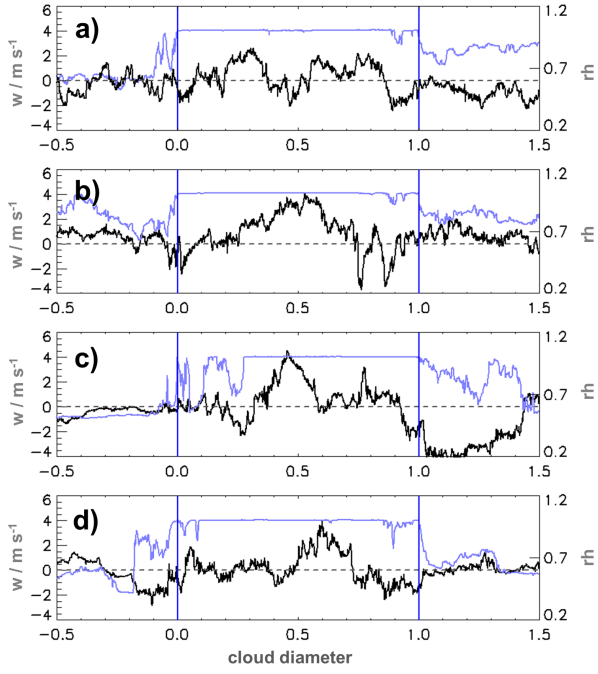

Figure 6. Relative humidity (blue line) and vertical wind (black line) for four alongwind directed cloud transects of an individual cloud during flight 2. The blue vertical lines indicate the cloud boundaries. The x-axis is scaled to the horizontal diameter of the cloud, where 0 marks the cloud edge on the upwind side and 1 the downwind edge. The data outside the cloud are shown for half a cloud diameter, each. The starttime of the transect, cloud length and height of the flight level are for panel (a) 12.27 UTC, 1043 m and 2620 ma.s.l., panel (b) 12.33 UTC, 1561 m and 2620 ma.s.l., panel (c) 12.40 UTC, 772 m and 2920 ma.s.l., panel (d) 12.42 UTC , 673 m and 2940 ma.s.l..

Atmos. Chem. Phys. Discuss., https://doi.org/10.5194/acp-2018-825
Manuscript under review for journal Atmos. Chem. Phys.
Discussion started: 5 October 2018

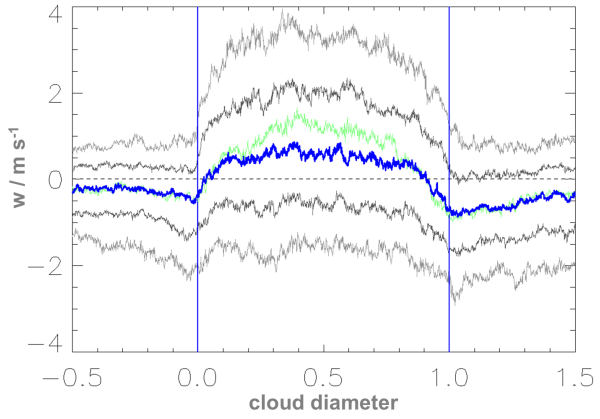

Figure 7. Distribution of the vertical wind speed of 191 cloud transects: median (blue line) $10, 25, 75$ and 90 percentiles (grey lines) with the scaling of the x-axis and the cloud boundaries as in Fig. 6. The individual cloud transects are scaled by the cloud length. The transects are arranged in a way that the upwind side is on the left and the crosswind transects are shown from left to right. The vertical blue lines indicate the cloud boundaries. The green solid line is the median of the vertical wind velocity for 94 selected cloud transects, which fulfill the stricter cloud requirements in Table 3.

Table 1. List of the measurement uncertainties for the main meteorological parameters of the sensors flown on the Caravan research aircraft. Results from Mallaun and Giez (2013)

Quantity	Variable	σ
Static air temperature	ts	0.15 K (0.5 K in clouds)
Humidity mixing ratio	mr	2 %(4 % below 0.5 g/kg)
Relative humidity	rh	3 %rh(5 %rh below 0.5 g/kg)
Dewpoint temperature	T_d	0.35 K (0.5 K in clouds)
Angle of attack	α	0.25°
Angle of sideslip	β	0.25°
Wind speed	ws	0.3 m/s
Wind angle	wa	2°
Alongwind component	u_f	0.3 m/s
Crosswind component	v_f	0.3 m/s
Vertical wind	w	0.25 m/s

Atmos. Chem. Phys. Discuss., https://doi.org/10.5194/acp-2018-825
Manuscript under review for journal Atmos. Chem. Phys.
Discussion started: 5 October 2018

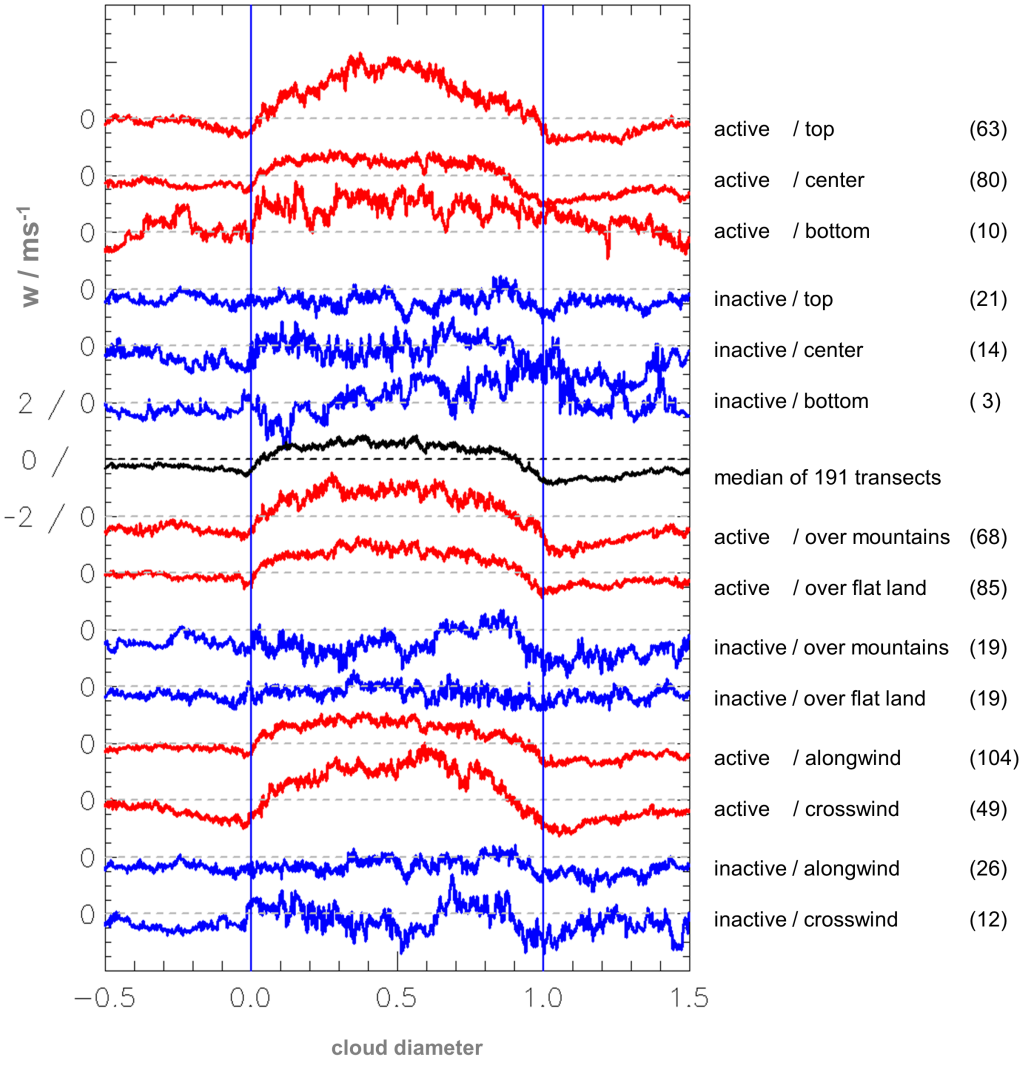

Figure 8. Median of the vertical wind for different transect heights, terrain, direction and activity status. The comparison is based on the 191 cloud transects shown in Fig. 7, with the same scaling of the x-axis. The red lines show active and the blue lines dissolving clouds. The detailed selection is explained on the right hand side of the respective line including the number of involved cases. For better readability the lines are vertically shifted and the grey dashed horizontal lines show the different 0 lines. Two adjacent 0 lines are separated by $2\,\mathrm{ms}^{-1}$

Atmos. Chem. Phys. Discuss., https://doi.org/10.5194/acp-2018-825
Manuscript under review for journal Atmos. Chem. Phys.
Discussion started: 5 October 2018

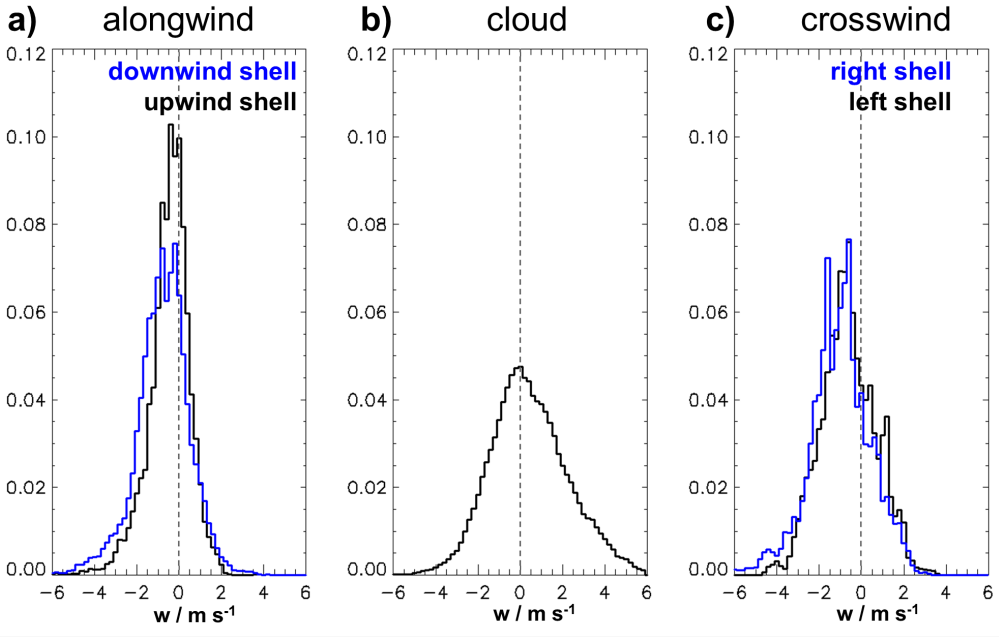

Figure 9. Distribution of the vertical wind in the cloud and shell regions for the 191 cloud transects. The three panels show the probability density function for a) the upwind shell and the downwind shell; b) the cloud and c) the right shell /left shell for the crosswind transects. For the distribution we set a bin size of $0.2\,\mathrm{ms}^{-1}$ and the results are scaled with the number of data points. The width of each shell is set to $20\,\%$ of the respective cloud diameter.

Table 2. Summary of flights conducted during the measurement campaigns in June 2012 and July 2013, with the number of cloud transects used in this study (191 total) and their pressure height measured in hecto feet.

number	date	time [UTC]	number of transects	flight levels [hft]	comment
1	10/07/2012	$12:30-14:58$	38	$75, 85, 95$	Cumulus with significant wind shear
2	26/07/2012	$8:15-10:45$	47	$75, 85, 100$	Cumulus with very weak wind ($\approx 2-4\,\mathrm{ms}^{-1}$) and dry surrounding
3	18/06/2013	$11:20-14:10$	30	$125, 140$	Cumulus above the alpine ridge
4	19/06/2013	$11:29-14:15$	35	$130, 140$	Cumulus above the alpine ridge
5	20/06/2013	$11:26-14:08$	22	$130, 140$	Cumulus above the alpine ridge
6	26/06/2013	$9:00-11:36$	19	65	Cloud streets and few isolated cumulus with moderate wind and high humidity

Atmos. Chem. Phys. Discuss., https://doi.org/10.5194/acp-2018-825
Manuscript under review for journal Atmos. Chem. Phys.
Discussion started: 5 October 2018

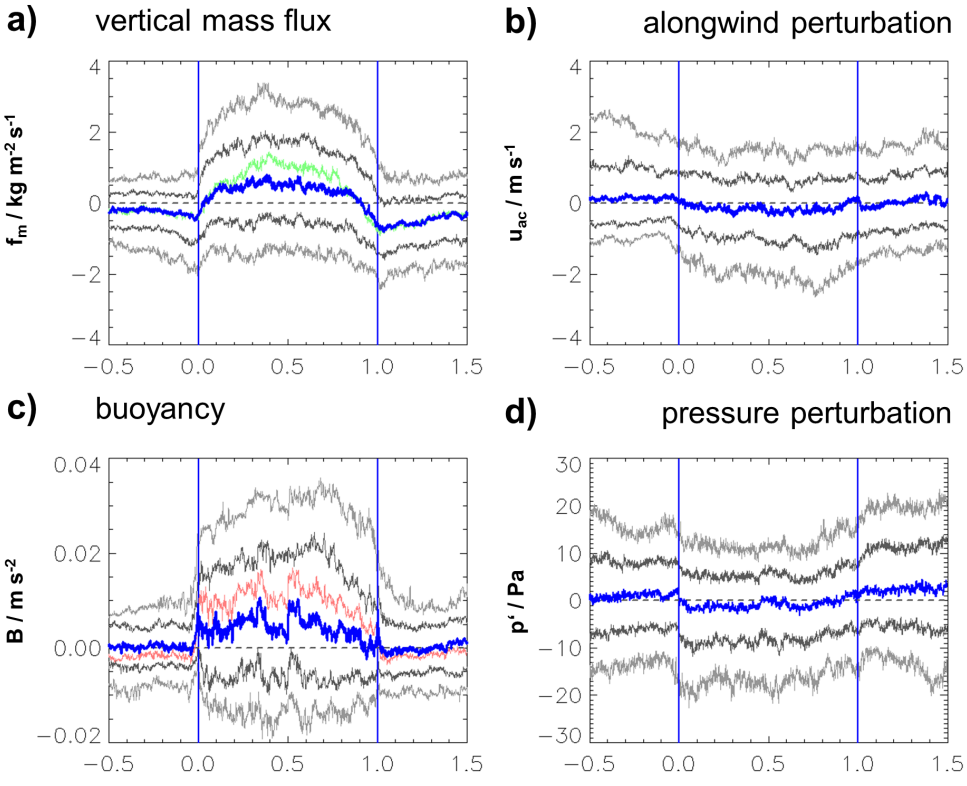

Figure 10. Same as Fig. 7 for the vertical mass flux (a), horizontal wind perturbation of the along flight path component (b), buoyancy (c) and the horizontal pressure perturbation (d). The red line in panel (c) is the median buoyancy calculated without the negative contribution of the LWC.

Atmos. Chem. Phys. Discuss., https://doi.org/10.5194/acp-2018-825
Manuscript under review for journal Atmos. Chem. Phys.
Discussion started: 5 October 2018

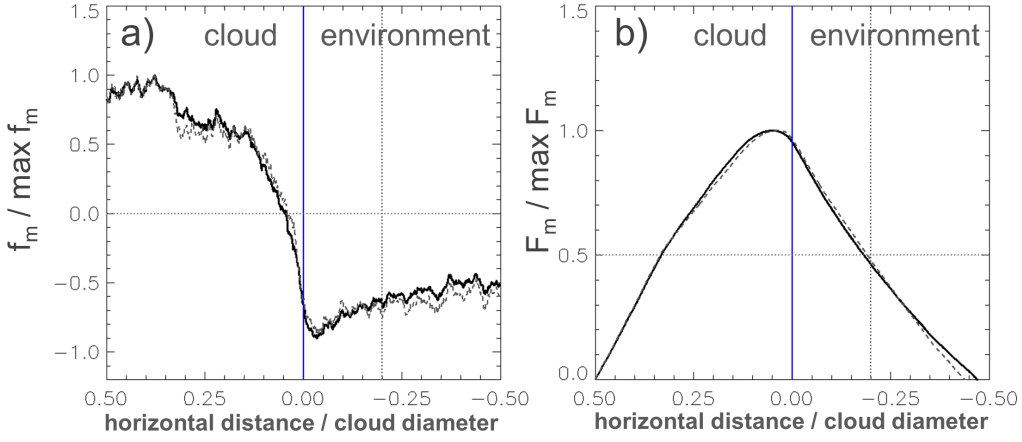

Figure 11. (a) Mean vertical mass flux (f_m) along 191 cloud transects scaled with the maximum mass flux. The x-axis is scaled with the cloud diameter. The grey dashed line shows the scaled f_m for 130 alongwind transects. (b) Integrated mass flux (F_m) from the center of the cloud (i.e., Eq. 7) scaled with the maximum value.

Table 3. Criteria for identifying the cloud and the subsiding shell. The stricter cloud requirements 4 and 5 are optional and used in a repetition of the analysis in order to test the sensitivity of the results.

	Cloud criteria:
1.	The cloud boundaries are defined by reaching humidity saturation.
2.	A cloud has a minimum diameter of 200 m.
3.	All parts of a single cloud possess a common cloud base, thus, a cloud transect can also contain regions of subsaturation (cloud gaps)
(4.	Any region of subsaturation (cloud gap) is shorter than 150 m.)
(5.	The cloud gaps may not cover more than 30 % of the cloud diameter)
	Minimum criteria for a subsiding shell:
1.	Outside the cloud a downdraft region exists with a length between 1 % and 20 % of the cloud diameter.
2.	The downdraft region starts within a distance of 5 % in cloud diameter away from the cloud border.
3.	The downdraft region inside the cloud starts no more than 20 % in cloud diameter away from the cloud border.

Atmos. Chem. Phys. Discuss., https://doi.org/10.5194/acp-2018-825
Manuscript under review for journal Atmos. Chem. Phys.
Discussion started: 5 October 2018

Atmospheric Chemistry and Physics Discussions

Table 4. Characteristics of the 191 (94) selected cloud transects as defined in Table 3. Numbers in parentheses are relative to the subset of 94 clouds with stricter limits on the cloud gaps. The transects are divided into legs along and cross to the main wind direction, into legs at the bottom, center or top of the cloud and the activity status. Active clouds have a positive mean buoyancy inside the cloud. Total numbers of cloud transects and transects which fulfill the criteria of a subsiding shell are listed.

	along	cross	flat land		mountain	
			active	inactive	active	inactive
total	130 (60)	61 (34)	85 (49)	19 (6)	68 (37)	19 (2)
shell	75 (33)	30 (14)	55 (34)	9 (1)	31 (12)	10 (0)

	bottom		center		top	
	active	inactive	active	inactive	active	inactive
total	10 (8)	3 (2)	80 (47)	14 (5)	63 (31)	21 (1)
shell	7 (5)	1 (0)	42 (22)	6 (1)	37 (19)	12 (0)

Table 5. Change of saturation dewpoint temperature in dependence of water vapor mixing ratio for different dewpoint temperatures (TS) and pressures (PS) during the measurement flights. The last column gives the estimated average value which is used for the temperature correction described in Sect. 2.4

flight	FL [hft]	PS [hPa]	TS [°C]	$\frac{\partial T_d}{\partial r}$ [K g^{-1}kg]	$\overline{\frac{\partial T_d}{\partial r}}$
	75	770	7	1.8	
1	85	735	5	1.9	2.0
	95	705	2	2.2	
	75	770	10	1.5	
2	85	735	8	1.6	1.6
	100	700	5	1.8	
	125	630	5	1.6	
3-5	130	625	4	1.7	1.8
	140	595	1	2.0	
6	65	800	2	2.5	2.5

Atmos. Chem. Phys. Discuss., https://doi.org/10.5194/acp-2018-825
Manuscript under review for journal Atmos. Chem. Phys.
Discussion started: 5 October 2018

Atmospheric Chemistry and Physics Discussions

Table 6. Distribution of sizes of the downdrafts just outside of the clouds for the 191 cloud transects. The left and right sides of the 61 crosswind transects are considered together. The percentages are measured relative to the cloud diameter. Only 29 cloud transects have a subsiding shell fulfilling the criteria in Table 3 on both sides and about half the transects have at least one subsiding shell.

	shell $1-20\,\%$	downdraft $>20\,\%$	no near downdraft	downdraft in cloud $>20\,\%$
upwind	59	43	19	9
downwind	39	58	23	10
crosswind	36	69	13	4

Table 7. Vertical wind speeds $[\mathrm{ms}^{-1}]$ of 191 selected cloud transects. The length of the cloud interior is variable and the shells are limited to $20\,\%$ of the cloud diameter. The table shows the mean vertical velocities, the median as well as the 25 and 75 percentiles.

	mean	25 percentile	median	75 percentile
cloud	$+0.5$	-0.7	$+0.4$	$+1.7$
upwind shell	-0.4	-0.9	-0.3	$+0.2$
downwind shell	-0.7	-1.4	-0.6	$+0.1$
crosswind shell	-0.8	-1.6	-0.7	$+0.2$